ChemistrySelect

ChemistrySelect
Chemistry Europe
European Chemical Societies Publishing

RESEARCH ARTICLE OPEN ACCESS

Discovery of Spirochromanone-Based Molecular Hybrids as Promising Anticancer Leads: An Integrated Experimental and Theoretical Study

Ramesh Reddy Mudda[1] | Rambabu Gundla[2] | Vikram Basava[1,3] | Baji Baba Shaik[4] | Vani Madhuri Velavalapalli[2] | Ramanaiah Chennuru[5] | Soňa Gurská[6] | Viswanath Das[6,7] | Naresh Kumar Katari[8,9]

[1]Department of Chemistry, GITAM School of Science, GITAM (Deemed to Be University), Bangalore, Karnataka, India | [2]Department of Chemistry, GITAM School of Science, GITAM (Deemed to Be University), Hyderabad, Telangana, India | [3]Chemical Immunology Laboratory, CIC bioGUNE, Basque Research and Technology Alliance (BRTA), Derio, Spain | [4]Department of Natural Products and Medicinal Chemistry, CSIR-Indian Institute of Chemical Technology, Hyderabad, India | [5]Centre of Excellence Polymorphism, Research and Development, Integrated Product Development (IPD), Cipla Ltd., Bangalore, Karnataka, India | [6]Institute of Molecular and Translational Medicine, Faculty of Medicine and Dentistry, Palacký University Olomouc, Olomouc, Czech Republic | [7]Czech Advanced Technologies and Research Institute (CATRIN), Institute of Molecular and Translational Medicine, Palacký University Olomouc, Olomouc, Czech Republic | [8]School of Chemistry & Physics, College of Agriculture, Engineering & Science, Westville Campus, University of KwaZulu-Natal, Durban, South Africa | [9]A&B Laboratories (An Amspec Group of Company), Houston, Texas, USA

Correspondence: Vikram Basava (vbasava@gitam.edu) | Viswanath Das (viswanath.das@upol.cz) | Naresh Kumar Katari (KatariN@ukzn.ac.za; dr.n.k.katari@gmail.com)

Received: 13 December 2025 | **Revised:** 4 June 2026 | **Accepted:** 5 August 2026

Keywords: ADMET | anticancer agents | spirochromanone | in silico

ABSTRACT

Cancer remains one of the leading causes of mortality worldwide, emphasizing the urgent need for the discovery of novel and selective chemotherapeutic agents. In this study, a new series of spirochromanone-based molecular hybrids was rationally designed and synthesized to explore their potential as anticancer agents. The synthesized compounds were fully characterized by spectroscopic techniques including NMR and LCMS. The in vitro cytotoxic evaluation of the synthesized hybrids against a panel of human cancer cell lines (A549, HCT116, U2OS, Jurkat, CCRF-CEM, MOLT-4, RAMOS, K562, MRC-5, and BJ cell lines) were assessed. Among all the compounds, **6b**, **6c**, **6g**, **6h**, and **6j** have been displayed promising inhibition against RAMOS cell lines with an IC_{50} range of 1.11–1.47 μM, respectively. In addition, compounds **6c**, **6j**, **6b**, and **6f** have been found to have potential inhibition against CCRF-CEM cell lines with an IC_{50} range of 7.71–13.55 μM. Furthermore, molecular docking studies were performed to explore the possible binding modes of the designed compounds within the active sites of ITK and BTK as a preliminary computational assessment. In silico ADMET analysis further supported the drug-like nature and acceptable pharmacokinetic profiles of the active hybrids.

1 | Introduction

Cancer is the second leading cause of death worldwide [1, 2]. Chemotherapy remains a major treatment in cancer diagnosis, but its lack of specificity leads to severe side effects and limited efficacy, while resistance development further reduces clinical success [3, 4]. These limitations underscore the need for novel agents with improved selectivity and potency [5, 6]. Liver cancer, in particular, poses a major global health challenge, with annual cases projected to exceed 1 million by 2025 (GLOBOCAN 2022) [7].

A comparison of the most recent global cancer statistics reported by the International Agency for Research on Cancer (IARC) shows a slight decrease in cancer-related mortality, from 10.0 million deaths in 2020 to 9.7 million in 2022, despite an increase in the number of new cases from 19.3 million to 20.0 million during the same period [8, 9]. This trend reflects advancements in cancer treatment and management. Nonetheless, success has been inconsistent among cancer types: while some, such as female breast and colorectal cancers, have shown only small gains, others, including lung and prostate cancers, have had a rise in mortality in 2022 compared to 2020 [10–12].

In recent years, considerable attention has been directed toward the discovery and development of novel anticancer agents with improved selectivity. In this context, significant efforts have been made to synthesize spiro-heterocyclic compounds with different chemotherapeutic potential [13–16]. Chromanone-based spirocyclic compounds have received special attention because they are found in a wide range of biologically active natural products, including alkaloids, vitamins, hormones, glycosides, and antibiotics, many of which are essential for human and animal health [17–20]. Over the last decade, significant progress has been made in the development of complex spiro-heterocyclic chroman-4-ones coupled with amido-piperidine scaffolds, which have demonstrated great potential and are routinely reported in both preclinical and clinical investigations [21–23]. Therefore, the increasing need for the synthesis of non-natural spirocyclic 4-oxo-chroman-piperidinamides has ignited a "gold rush" in academia and industry. Varasi et al. identified novel spirochromone-2,4-piperidine derivatives as promising HDAC inhibitors (**1**) and tested their antiproliferative activity against a variety of cancer cell lines [24]. Abdelatef et al. reported spirochromanone derivatives with a phenyl sulfonamide spacer (**2**), which showed IC_{50} values ranging from 0.31 to 5.62 μM against MCF-7, A2780, and HT-29 cancer cells (Figure 1) [25]. In the other hand, the sulfonamide moiety serves as an effective bioisostere of the carboxylic acid group, capable of forming similar hydrogen-bonding interactions while overcoming drawbacks such as metabolic instability, toxicity, and poor membrane permeability [26, 27]. Many sulfonamide derivatives exhibit potent anticancer activity, and several have been FDA-approved, including **Belinostat** (an HDAC inhibitor for T-cell lymphoma) [28] and **ABT-199** (Venetoclax), a selective Bcl-2 inhibitor for chronic lymphocytic leukemia [29]. Additionally, compounds like **pazopanib** demonstrate VEGFR-2 inhibition, underscoring the sulfonamide group's broad therapeutic relevance in cancer treatment (Figure 1) [30].

2 | Results and Discussion

2.1 | Chemistry

The target compounds were synthesized through a three-step procedure, as shown in Scheme 1. First, the reaction of substituted salicylaldehyde **1** with cyclic β-ketoamides **2** in the presence of pyrrolidine in methanol afforded the corresponding spirochromanone derivatives (**3**), followed by Boc-deprotection with trifluoroacetic acid in led to the formation of the trifluoroacetate salts (**4**). Finally, coupling of intermediates (**4**) with sulfonyl chloride (**5**) in furnished the desired spirochromanone-piperidinamide conjugates.

All the synthesized intermediates and final compounds were characterized and confirmed by ^{1}H NMR and LC-MS analysis. Formation of spiro compound in stage-1 can be confirmed by appearance of chemical shift at 7.87–6.49 ppm as multiplate and doublets due to aromatic protons; methylene protons could be found at 4.09–1.56 as doublets and multiplets; singlet at 2.71–2.69 refers methylene protons adjacent to the ketonic group in 3-lactone ring. Singlet of nine protons at 1.45–1.46 indicates "*N*-Boc" protons. In stage-2, obtained intermediate was confirmed with mass data and moved ahead to the step with above 98% of LC purity. In the final stage, the aromatic protons of product(s) appear as doublet and multiplet at 8.51–6.08; —NH— proton signals at around 6.22 as singlet. Methyl group on oxo-pyrrolidine ring appears as singlet at 2.03–2.05. —CH_3 of ethyl group on oxo-pyrrolidine ring as triplet at 1.05–1.04. MS (ESI^+) data also stood as confirmation support along with LC purity.

2.2 | Anticancer Activity

All the synthesized compounds were screened for in vitro cytotoxic activity by 3-(4,5-dimethylthiazol-2-yl)-5-(3-carboxymethoxyphenyl)-2-(4-sulfophenyl)-2*H*-tetrazolium (MTS) assay against A549, HCT116, U2OS, Jurkat, CCRF-CEM, MOLT-4, RAMOS, K562, MRC-5, and BJ cell lines and the obtained results were presented in Table 1.

It is observed that almost all the compounds were inactive against A549, HCT116, U2OS, K562, MRC-5, and BJ cell lines and found IC_{50} of > 50 μM. Compound **6h** alone exhibited potential activity against MOLT-4 cell line with an IC_{50} of 10.69 μM. Against, Jurkat cell line, compound **6f** and **6h** were exhibited promising activity with and IC_{50} of 8.2 and 10.37 μM, respectively. Further, compounds **6a**, **6i**, and **6j** were exhibited with good inhibition with IC_{50} range of 11.32–13.36 μM. Further, compound **6k** exhibited the most promising activity against CCRF-CEM and RAMOS cell lines with an IC_{50} of 1.21 μM.

Of all the compounds, **6c**, **6j**, **6b**, and **6f** have been displayed potent inhibition with an IC_{50} of 9.39 μM, 10.95, 12.58, and 13.55 μM and 7.71 μM against CCRF-CEM cell lines and remaining compounds showed moderate activity with an IC_{50} range of 15.29–27.86 μM. Further with strong potency, compounds **6b**, **6c**, **6g**, **6h**, and **6j** exhibited 1.11, 1.01, 1.38, 1.47, and 1.37 μM possess more selectivity toward RAMOS cells.

2.3 | In Silico Investigation

2.3.1 | Pharmacokinetic Properties

The Physico–chemical pharmacokinetic and drug-likeness properties analyzed by Swiss ADME software [31]. Enhanced paracellular and transcellular absorption qualities, as well as an impact on clearance, which leads to improved renal excretion, and mild toxicity are anticipated for low molecular weight and lipophilic compounds [32, 33]. Drug-like molecules (DLMs) are defined as molecules that meet the "rule of 5" (Ro5). A molecule which complies with the Ro5 criteria has a molecular mass of less than 500, a logP of less than 5, and fewer than 5 and 10 hydrogen bond

TABLE 1 | Anticancer activity results of the synthesized titled compounds (**6a–l**).

Compound code	Chemical structure	IC_{50} (μM)									
		ITK/BTK null			ITK high cells			BTK high cells		Non-cancer cells	
		A549	HCT 116	U2OS	Jurkat	CCRF-CEM	MOLT-4	RAMOS	K562	MRC-5	BJ
6a	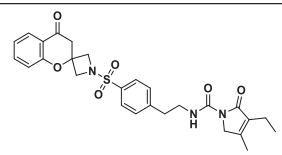	> 50	> 50	> 50	**11.32 ± 1.13**	19.03 ± 4.54	> 50	3.56 ± 0.82	> 50	> 50	> 50
6b	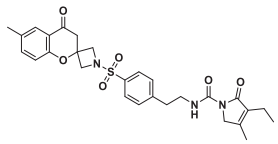	> 50	> 50	> 50	> 50	**12.58 ± 2.86**	> 50	**1.11 ± 0.29**	> 50	> 50	> 50
6c	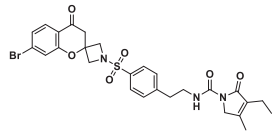	> 50	> 50	> 50	> 50	**9.39 ± 0.78**	> 50	**1.01 ± 0.069**	> 50	> 50	> 50
6d	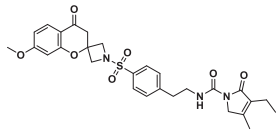	> 50	> 50	> 50	21.21 ± 3.49	15.29 ± 2.25	> 50	2.76 ± 0.79	> 50	> 50	> 50
6e	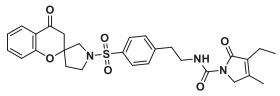	> 50	> 50	> 50	18.15 ± 4.08	19.89 ± 3.58	> 50	4.93 ± 1.06	> 50	> 50	> 50
6f	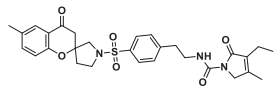	> 50	> 50	> 50	**8.2 ± 2.02**	**13.55 ± 2.96**	> 50	> 50	> 50	> 50	> 50
6g	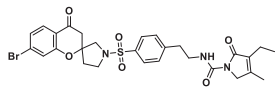	> 50	> 50	> 50	24.22 ± 4.17	24.22 ± 4.17	> 50	**1.38 ± 0.24**	> 50	> 50	> 50
6h	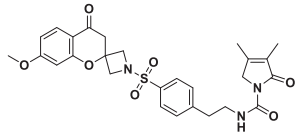	> 50	> 50	> 50	**10.37 ± 0.79**	15.29 ± 2.25	10.69 ± 0.51	**1.47 ± 0.36**	> 50	> 50	> 50

(Continues)

TABLE 1 | (Continued)

Compound code	Chemical structure	IC_{50} (μM)									
		ITK/BTK null			ITK high cells			BTK high cells		Non-cancer cells	
		A549	HCT 116	U2OS	Jurkat	CCRF-CEM	MOLT-4	RAMOS	K562	MRC-5	BJ
6i	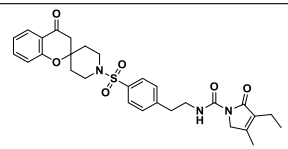	> 50	> 50	> 50	**12.04 ± 2.64**	27.86 ± 5.64	> 50	3.35 ± 0.74	> 50	> 50	> 50
6j	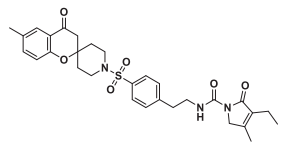	> 50	> 50	> 50	**13.36 ± 3.11**	**10.95 ± 2.02**	> 50	**1.37 ± 0.26**	> 50	> 50	> 50
6k	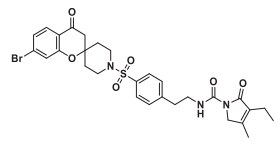	> 50	> 50	> 50	> 50	**1.21 ± 0.12**	> 50	**1.21 ± 0.12**	> 50	> 50	> 50
6l	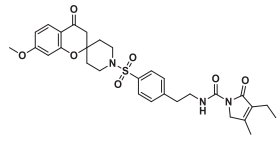	> 50	> 50	> 50	47.27 ± 3.86	> 50	> 50	> 50	> 50	> 50	> 50
	Ibrutinib	29.35 ± 3.40	29.82 ± 0.68	22.61 ± 3.06	5.15 ± 0.70	4.25 ± 0.93	5.26 ± 0.65	0.29 ± 0.04	27.36 ± 3.24	27.86 ± 0.48	28.91 ± 1.31

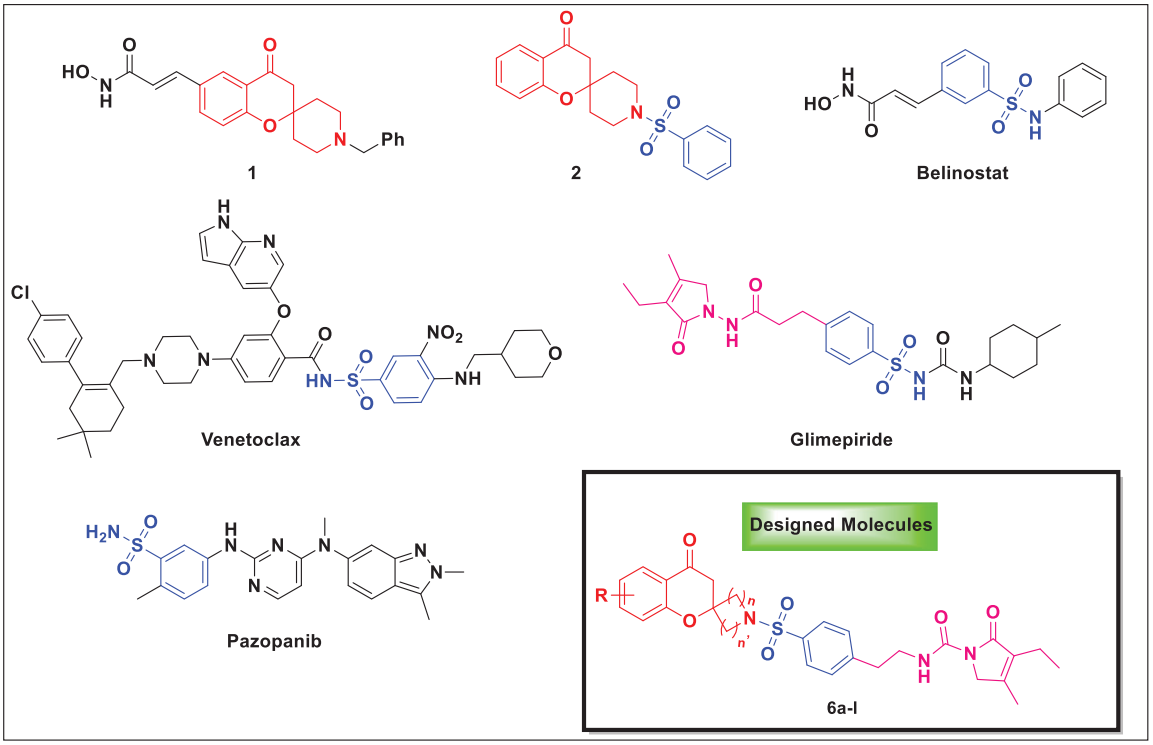

FIGURE 1 | Scaffold design strategy for new ITK and BTK inhibition.

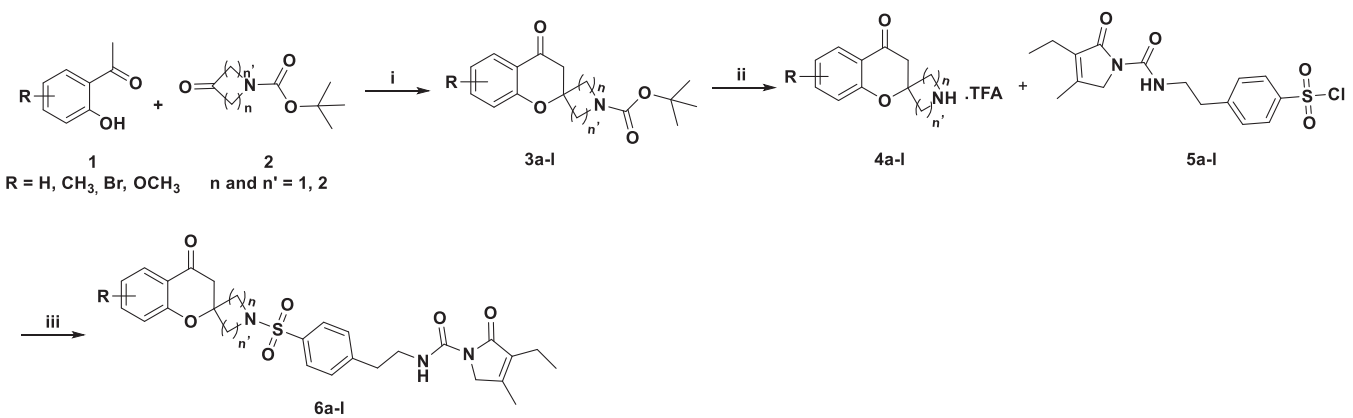

SCHEME 1 | Synthetic route of targeted compounds **6a–l**. Reagent and conditions: (i) Pyrrolidine, MeOH, 50°C, 16 h; (ii) trifluoroacetic acid, DCM, 0°C-rt, 1 h; (iii) Et_3N, DCM, °C-rt, 16 h.

donors and acceptors, respectively [34]. Compounds with rotatable bonds, polar surface area, and H-bond donors and acceptors that are equal to or less than 10, 140, and 12 have higher oral bioavailability, according to the Veber rule [35]. These properties additionally assist in the creation of compounds with enhanced absorption, distribution, metabolism, excretion, and toxicity (ADMET) [36, 37]. Because of this, a molecule's physicochemical characteristics and the degree to which they are carefully regulated now have a big impact on whether it can be used as a therapeutic candidate and how effectively it works during crucial phases of drug development. The elements resulted in the formation of carbamide and spirochromanone molecular hybrids that adhered to DLM nature but had distinct structural and functional changes.

The SwissADME tool was used to evaluate the physicochemical, pharmacokinetic, and drug-likeness properties of compounds **6a–l** (Table 2, Figures 2 and 3). The molecular weights ranged from 523.60 to 630.55 Da, indicating that all compounds exceed the molecular weight criterion (< 500 Da) defined in Lipinski's rule of five and resulting in one Lipinski violation for most compounds, while compound **6h** showed two violations. The compounds possessed seven to nine hydrogen-bond acceptors, one hydrogen-bond donor and eight to nine rotatable bonds, indicating acceptable hydrogen-bonding capacity and moderate molecular flexibility. The calculated topological polar surface area (TPSA) values (121.47–139.93 Å ranged from 121.47 to 139.93 $Å^2$, which are generally compatible with oral absorption but may reduce passive membrane permeability for some derivatives with

TABLE 2 | The physicochemical pharmacokinetic and drug-likeness characteristics Spirochromanone molecular hybrids.

Property	6a	6b	6c	6d	6e	6f	6g	6h	6i	6j	6k	6l
MW	523.6	537.63	602.5	553.63	537.63	551.65	616.52	569.63	551.65	565.68	630.55	581.68
#Heavy atoms	37	38	38	39	38	39	39	40	39	40	40	41
#Aromatic heavy atoms	12	12	12	12	12	12	12	12	12	12	12	12
Fraction Csp3	0.37	0.39	0.37	0.39	0.39	0.41	0.39	0.39	0.41	0.43	0.41	0.43
#Rotatable bonds	8	8	8	9	8	8	8	9	8	8	8	9
#H-bond acceptors	7	7	7	8	7	7	7	9	7	7	7	8
#H-bond donors	1	1	1	1	1	1	1	1	1	1	1	1
MR	144.02	148.99	151.72	150.51	148.83	153.79	156.53	151.60	153.64	158.6	161.34	160.13
TPSA	121.47	121.47	121.47	130.7	121.47	121.47	121.47	139.93	121.47	121.47	121.47	130.7
iLOGP	2.62	2.99	3.31	2.59	2.98	3.34	3.67	2.64	3.34	3.7	4.03	3.31
XLOGP3	3.24	3.54	4.0	3.24	3.63	3.93	4.39	3.18	4.02	4.32	4.78	4.02
WLOGP	1.32	1.52	1.89	1.02	1.52	1.72	2.08	0.66	1.72	1.91	2.27	1.41
MLOGP	2.83	3.37	3.52	2.92	3.07	3.61	3.75	2.51	3.31	3.85	3.99	3.39
Consensus Log P	−4.45	−4.76	−5.37	−4.54	−4.76	−5.06	−5.67	−4.66	−5.06	−5.37	−5.98	−5.15
ESOL Solubility (mg/ml)	1.86E-02	9.29E-03	2.59E-03	1.60E-02	9.42E-03	4.76E-03	1.316E-03	1.24E-02	4.76E-03	2.40E-03	6.57E-04	4.08E-03
ESOL Solubility (mol/l)	3.56E-05	1.73E-05	4.30E-06	2.90E-05	1.75E-05	8.63E-06	2.12E-06	2.17E-05	8.63E-06	4.24E-06	1.04E-06	7.01E-06
ESOL Class	Moderately soluble	Moderately soluble	Moderately soluble	Moderately soluble	Moderately soluble	Moderately soluble	Moderately soluble	Moderately soluble	Moderately soluble	Moderately soluble	Moderately soluble	Moderately soluble
Ali Log S	−4.82	−5.2	−5.54	−4.98	−5.19	−5.57	−5.91	−5.23	−5.57	−5.94	−6.28	−5.73
Ali Solubility (mg/ml)	7.9 E-03	3.35E-03	1.75E-03	5.75E-03	3.44E-03	1.49E-03	7.58E-03	3.36E-03	1.49E-03	6.47E-04	3.28E-04	1.08E-03
Ali Solubility (mol/l)	1.51E-05	6.24E-06	2.90E-06	1.04E-05	6.39E-06	2.70E-06	1.23E-06	5.904E-05	2.70E-06	1.14E-06	5.20E-07	1.86E-06
Ali Class	Moderately soluble	Moderately soluble	Moderately soluble	Moderately soluble	Moderately soluble	Moderately soluble	Moderately soluble	Moderately soluble	Moderately soluble	Moderately soluble	Poorly soluble	Moderately soluble
Silicos-IT LogSw	−7.26	−7.63	−8.02	−7.35	−7.53	−7.89	−8.28	−7.07	−7.79	−8.16	−8.54	−7.88

(Continues)

TABLE 2 | (Continued)

Property	6a	6b	6c	6d	6e	6f	6g	6h	6i	6j	6k	6l
Silicos-IT Solubility (mg/ml)	2.86E-05	1.25E-05	5.82E-06	2.45E-05	1.61E-05	7.03E-06	3.27E-06	4.80E-05	9.01E-06	3.95E-06	1.84E-06	7.74E-06
Silicos-IT Solubility (mol/l)	5.46E-08	2.33E-08	9.66E-09	4.43E-08	2.99E-08	1.27E-08	5.31E-08	8.43E-08	1.63E-08	6.98E-09	2.92E-09	1.33E-08
Silicos-IT class	Poorly soluble	Poorly soluble	Poorly soluble	Poorly soluble	Poorly soluble	Poorly soluble	Poorly soluble	Poorly soluble	Poorly soluble	Poorly soluble	Poorly soluble	Poorly soluble
GI absorption	High	High	High	High	High	High	High	Low	High	High	Low	Low
BBB permeant	No	No	No	No	No	No	No	No	No	No	No	No
Pgp substrate	Yes	Yes	Yes	Yes	Yes	Yes	Yes	Yes	Yes	Yes	Yes	Yes
CYP1A2 inhibitor	No	No	No	No	No	No	No	No	No	No	No	No
CYP2C19 inhibitor	No	No	No	No	No	No	No	No	No	No	No	No
CYP2C9 inhibitor	Yes	Yes	Yes	Yes	Yes	Yes	Yes	Yes	Yes	Yes	Yes	Yes
CYP2D6 inhibitor	No	No	No	No	No	No	No	No	No	No	No	No
CYP3A4 inhibitor	Yes	Yes	Yes	Yes	Yes	Yes	Yes	Yes	Yes	Yes	Yes	Yes
log Kp (cm/s)	−7.63	−7.46	−7.63	−7.84	−7.46	−7.29	−7.46	−7.9	−7.29	−7.12	−7.29	−7.5
Lipinski #violations	1	1	1	1	1	1	1	2	1	1	1	1
Ghose #violations	2	2	2	2	2	3	2	3	3	3	3	3
Veber #violations	0	0	0	0	0	0	0	1	0	0	0	0
Egan #violations	0	0	1	0	0	0	1	0	0	0	1	0
Muegge #violations	0	0	1	0	0	0	0	0	0	0	1	0
Bioavailability Score	0.55	0.55	0.55	0.55	0.55	0.55	0.55	0.17	0.55	0.55	0.55	0.55
PAINS #alerts	0	0	0	0	0	0	0	0	0	0	0	0
Brenk #alerts	0	0	0	0	0	0	0	0	0	0	0	0
Leadlikeness #violations	2	2	2	2	2	2	3	2	2	3	3	2
Synthetic Accessibility	4.98	5.1	5.02	5.17	5.14	5.27	5.19	5.51	5.13	5.26	5.18	5.33

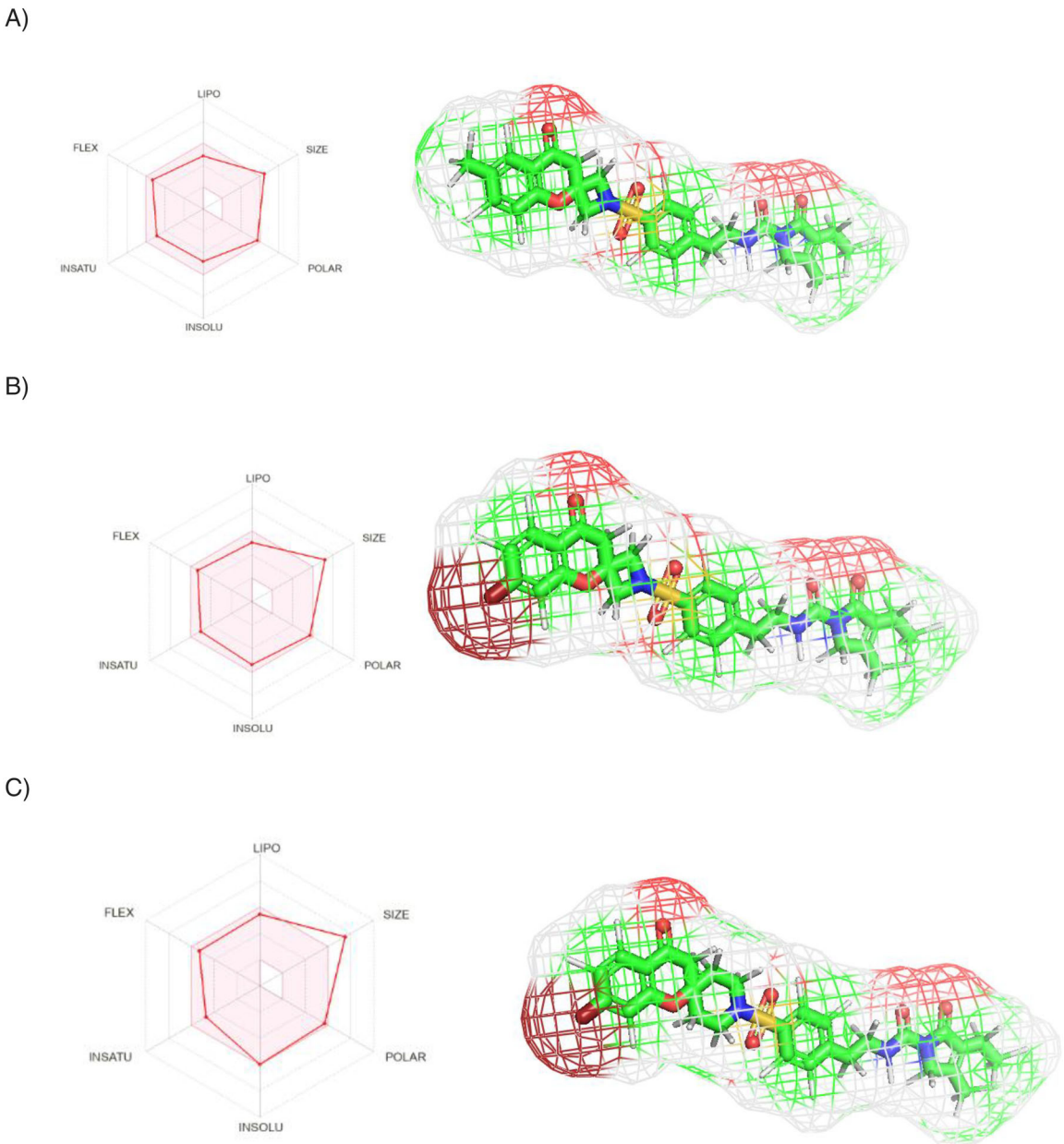

FIGURE 2 | The figure represents the physicochemical properties of the compounds (a) **6b**, (b) **6c**, and (c) **6k** compounds.

higher polarity. The compounds exhibited moderate predicted lipophilicity based on individual log*P* descriptors, suggesting a balance between hydrophobicity and polarity that may support membrane interaction while avoiding excessive lipophilic burden. Solubility prediction using ESOL, Ali, and Silicos-IT models suggested moderate to poor aqueous solubility, particularly for compounds with higher molecular weight.

Pharmacokinetic prediction indicated that most compounds demonstrated high predicted GI absorption, whereas **6h**, **6k**, and **6l** showed lower absorption. None of the compounds were predicted to penetrate the blood–brain barrier (BBB). All compounds were predicted to be P-glycoprotein (P-gp) substrates, which may reduce intracellular exposure and influence bioavailability. Additionally, all derivatives showed predicted inhibition of CYP2C9 and CYP3A4, while no inhibition was predicted for CYP1A2, CYP2C19, or CYP2D6. Drug-likeness analysis showed 2–3 Ghose violations and 2–3 lead-likeness violations across the series. Most compounds displayed a bioavailability score of 0.55, except **6h** (0.17). No PAINS or Brenk alerts were detected, and synthetic accessibility scores (4.98–5.51) suggested moderate synthetic feasibility. Overall, the compounds demonstrated acceptable predicted ADME characteristics; however, the observed molecular weight, predicted P-gp substrate behavior, and CYP inhibition profiles indicate areas for future structural optimization.

2.3.2 | Molecular Docking

In silico molecular docking studies on ITK and BTK were conducted to illustrate the mechanism of anticancer activity and to gain information about the binding affinity and intermolecular

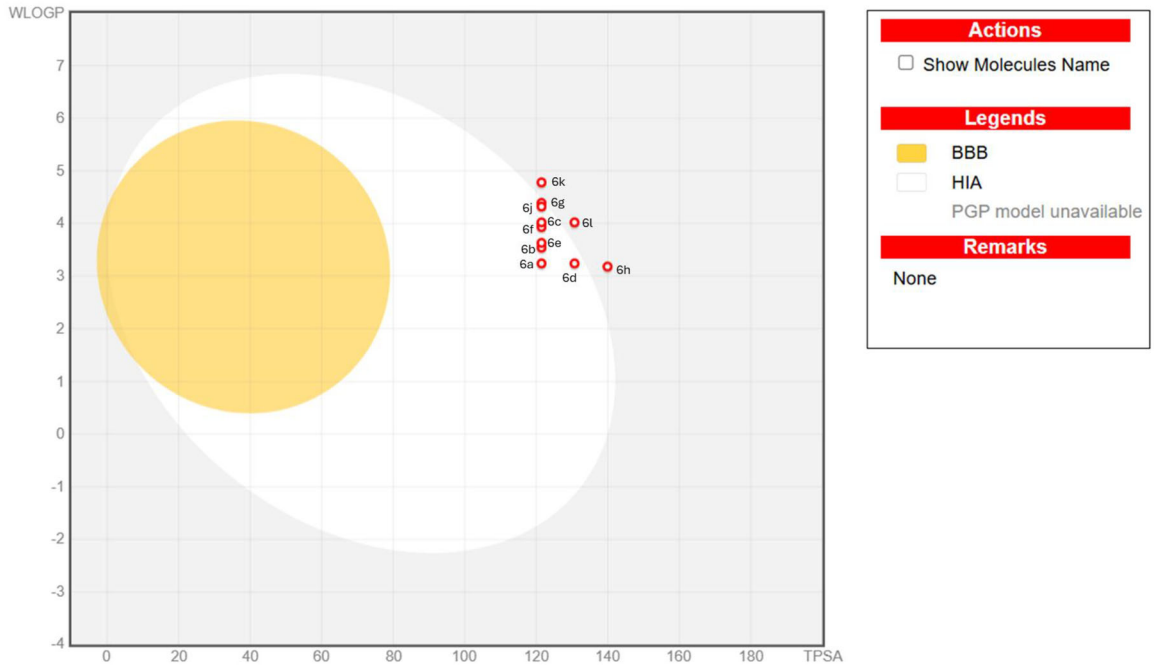

FIGURE 3 | BOILED Egg model of the designed and synthesized molecules.

TABLE 3 | Docking scores of the synthesized compounds with ITK (**PDB: 4M15**) and BTK (**PDB: 5P9J**) protein.

S. no	Compound	ITK docking score (Kcal/mol)	BTK docking score (Kcal/mol)
1	6a	−9.7	−11.0
2	6b	−9.8	**−11.1**
3	6c	−10	**−10.9**
4	6d	−9.3	−9.6
5	6e	−9.9	−10.4
6	6f	−9.8	−10.8
7	6g	**−10.1**	−10.2
8	6h	−9.6	−10.7
9	6i	−10.5	−10.8
10	6j	**−10.5**	−10.9
11	6k	**−10.2**	**−11.0**
12	6l	−9.8	−10.3
13	Co-Crystal	−8.5	−9.1

interactions of the newly synthesized compounds with the target's active sites to better understand the likely mechanism by which these recently developed spiro compounds could exhibit their anticancer activity. The compounds that docked to the target protein's active site pocket were categorized based on their binding energies, as shown in Table 3. The compound **6g**, **6j**, and **6k** showed docking scores of −10.1, −10.5, and −10.2 kcal/mol, respectively for ITK protein whereas co-crystal showed -8.5 kcal/mol. The compounds **6b**, **6c**, and **6k** showed docking scores of −11.1, −10.9, and −11.0 kcal/mol, respectively for BTK protein whereas standard drug showed −9.1 kcal/mol.

2.3.2.1 | Interactions of Compounds With Protein ITK. Compound **6g** formed the Vander Waals interaction with amino acids ASN A-564, SER A-371, TYR A-512, GLY A-441, GLU A-439, MET A-438, ARG A-486 (Figure 4). The Carbon–hydrogen interactions are with amino acids GLN A-373, GLY A-372, LYS A-391, and Pi-sigma with ILE A-369. The alkyl and Pi–alkyl interactions are with LYS A-519, TRP A-524, LYS A-523, CYS A-442, LEU A-489, PHE A-437, and ALA A-389 amino acids. The compound **6j** (Figure 5) showed Vander Waals interactions with amino acids ASN A-564, MET A-438, TYR A-524, GLY A-441, LYS A-391, ARG A-448. The hydrogen bond and Pi–sulfur interactions are with amino acid CYS A-442. The alkyl and

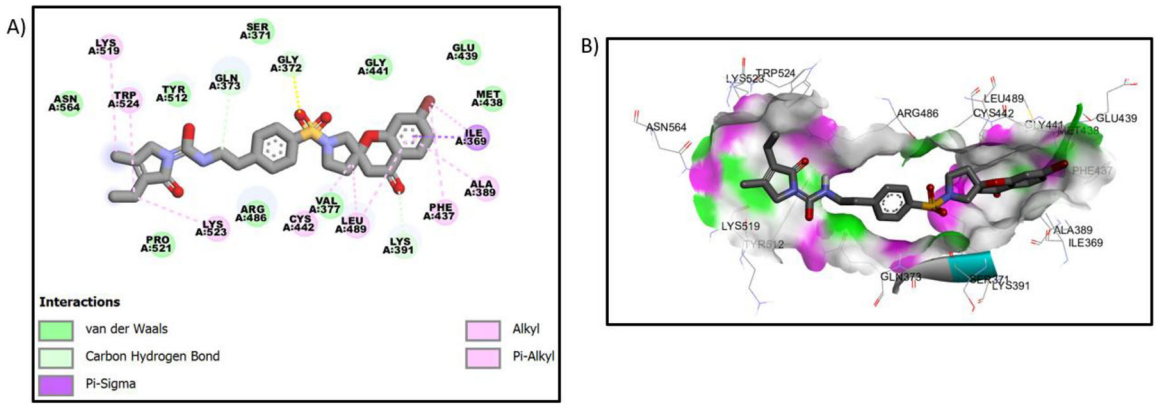

FIGURE 4 | (A) **6g** Interaction image with 4M15 protein and (B) **6g** showing hydrogen bond acceptor (green) and donor (pink).

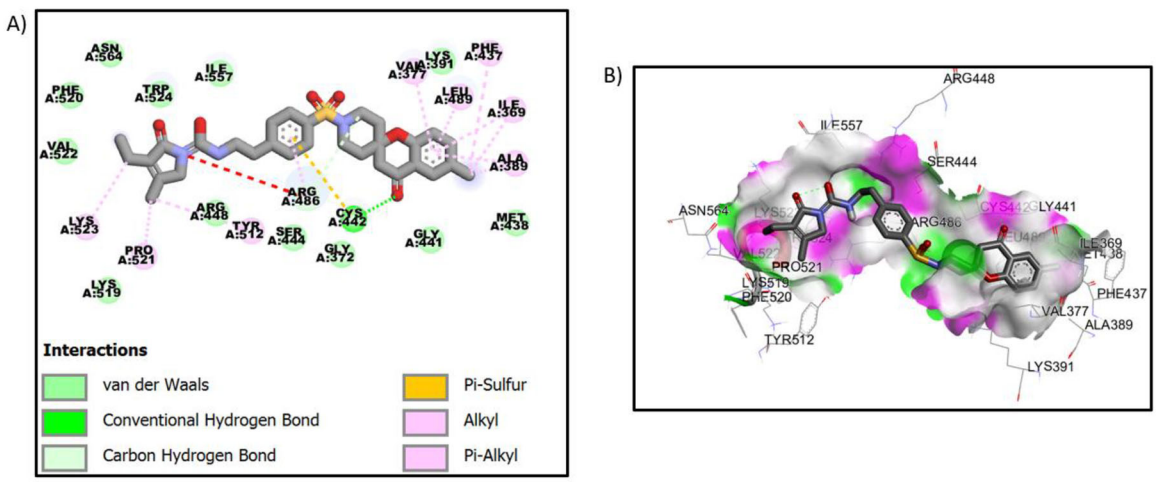

FIGURE 5 | (A) **6j** Interaction image with 4M15 protein and (B) **6j** showing hydrogen bond acceptor (green) and donor (pink).

Pi–alkyl interactions are with VAL A-377, PHE A-437, LYS A-523, LEU A-489, ILE A-369, TYR A-512, PRO A-521, and ALA A-389 amino acids. Next compound **6k** showed Vander Waals interactions with amino acids ASP A-445, MET A-438, GLN A-373, GLY A-441, SER A-371, GLU A-436. The hydrogen bond interactions are with amino acid ASN A-487 and ARG A-486. The alkyl and Pi–alkyl interactions are with VAL A-377, PHE A-437, LYS A-523, LEU A-489, ILE A-369, TYR A-512, PRO A-521, and ALA A-389 amino acids and carbon hydrogen interaction is with GLY A-375. The alkyl and alkyl–Pi interactions are with ILE A-369, VAL A-377, LEU A-489, MET A-503, PHE A-374, VAL A-507, CYS A-442, AND Pi anion interaction with ASP A-500. Of all the compounds, compound **6k** (Figure 6) showed required interactions with the protein ITK. The cocrystal representation was shown in Figure 7.

2.3.2.2 | Interactions of Compounds With Protein BTK.

The compound **6b** (Figure 8) showed hydrogen bond interactions with SER A-538 and Vander Waals interactions with CYS A-481, TYR A-476, MET A-477, VAL A-458, LYS A-430, THR A-474, LEU A-460, ASN A-479, GLU A-488. The Pi sigma interaction is with LEU A-528 and the alkyl interactions are with amino acids ALA A-428, VAL A-416, LEU A-408, MET A-449, PHE A-540, PHE A-442, LEU A-542, ILE A-472. Similarly, compound **6c** (Figure 9) demonstrated key hydrogen bonds with THR A-410, ASN A-526, LYS A-558 and Vander Waals interactions with SER A-543, VAL A-546, ARG A-525, GLY A-409, LYS A-430, SER A-538, THR A-474, GLU A-475, MET A-477, TYR A-476, GLY A-480, LEU A-408, CYS A-481, GLY A-411, GLN A-412, and ASP A-521. The alkyl interactions are shown with amino acids LEU A-542, ALA A-428, TYR A-551, VAL A-416, VAL A-458, and Pi–Sigma interactions with LEU A-528. Furthermore, compound **6k** (Figure 10) displayed Vander Waals interactions with SER A-543, TYR A-551, GLN A-412, ASN A-526, ASP A-539, GLY A-411, GLY A-480, MET A-477, LYS A-430, SER A-558, ARG A-525, LYS A-558. The Pi–sigma bond is formed with amino acid LEU A-528 and alkyl Pi interactions with PRO A-560, PHE A-574, PHE A-559, LEU A-408. The Pi–cation interactions are with amino acids ASP A-521 and the carbon hydrogen bond with THR A-552 amino acid. The reference drug Ibrutinib Interaction was shown in Figure 11.

3 | Conclusion

A series of Spirochromanone-based hybrids were designed, synthesized and evaluated for their in vitro anticancer activities against A549, HCT116, U2OS, Jurkat, CCRF-CEM, MOLT-4, RAMOS, K562, MRC-5, and BJ cell lines. Several compounds

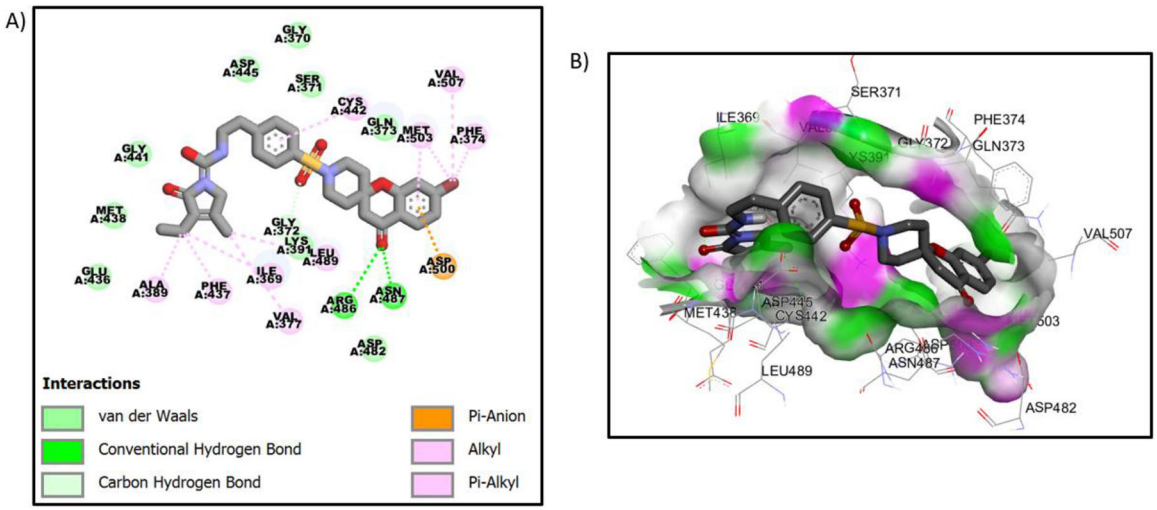

FIGURE 6 | (A) **6k** Interaction image with 4M15 protein and (B) **6k** showing hydrogen bond acceptor (green) and donor (pink).

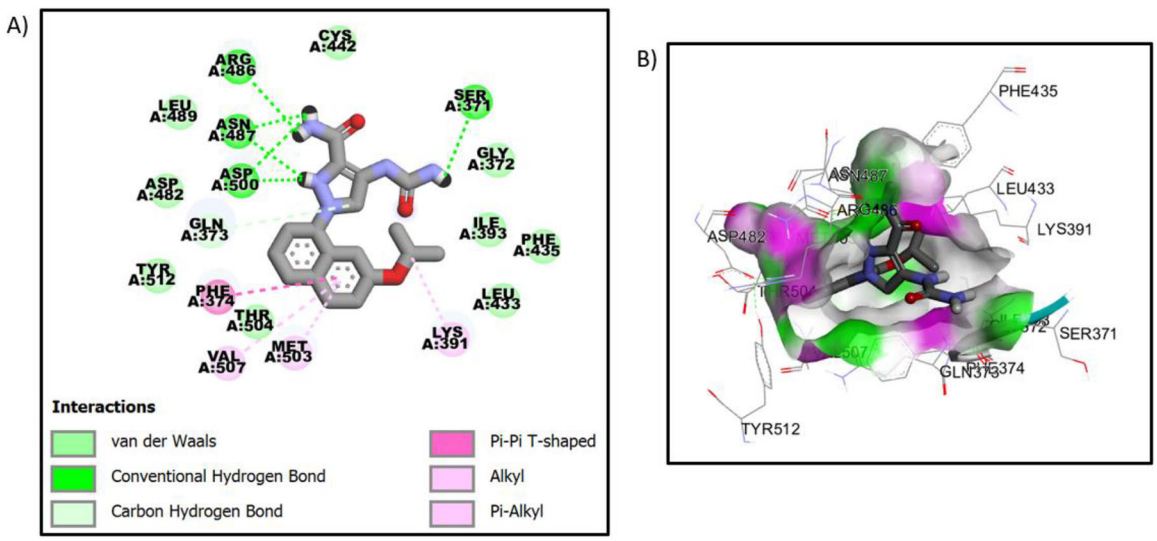

FIGURE 7 | (A) Co-crystal Interaction image and (B) co-crystal showing hydrogen bond acceptor (green) and donor (pink) interactions.

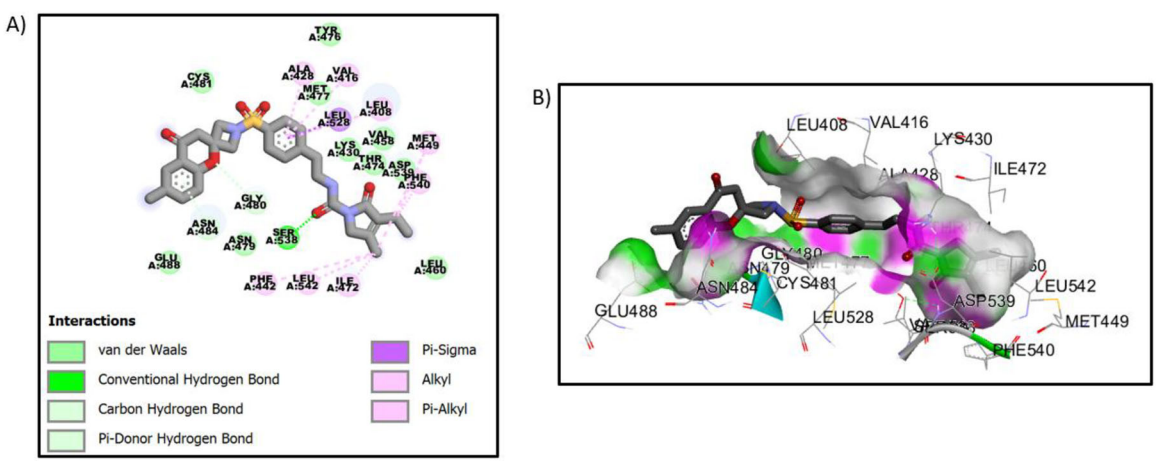

FIGURE 8 | (A) **6b** Interaction image with Protein 5P9J and (B) **6b** showing hydrogen bond acceptor (green) and donor (pink).

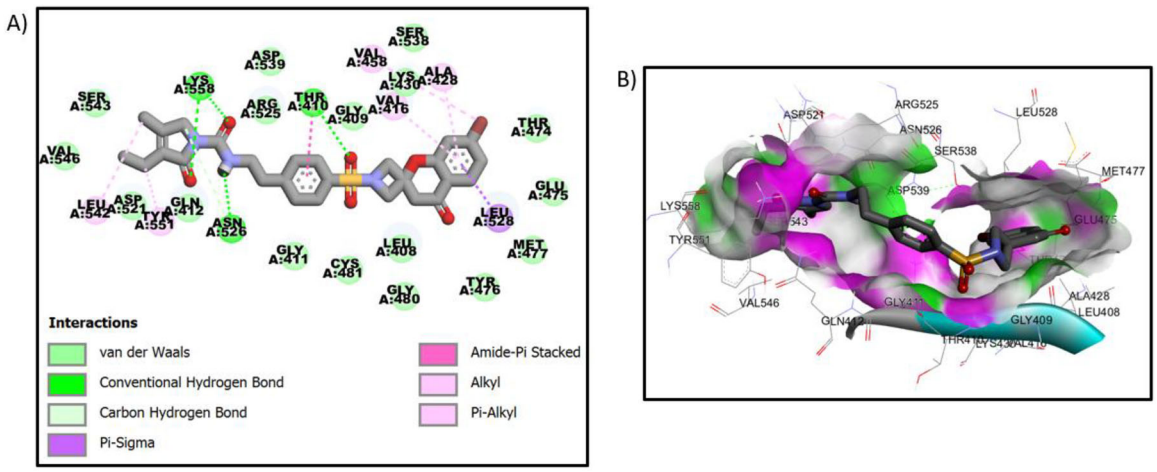

FIGURE 9 | (A) **6c** Interaction image with Protein 5P9J and (B) **6c** showing hydrogen bond acceptor (green) and donor (pink).

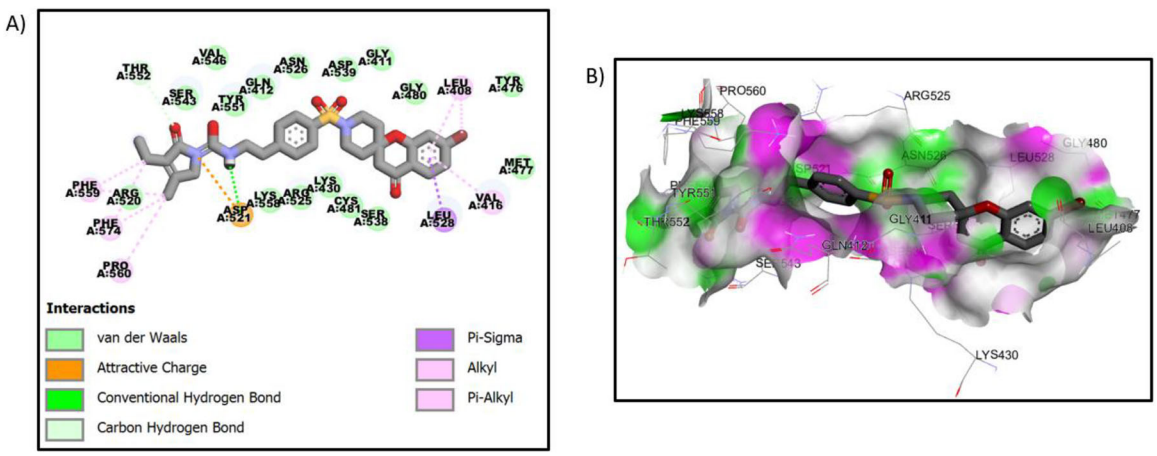

FIGURE 10 | (A) **6k** Interaction image with Protein 5P9J and (B) **6k** showing hydrogen bond acceptor (green) and donor (pink).

were displayed promising activity against Jurkat, CCRF-CEM, and RAMOS cell lines. Among all, compound **6c** displayed promising activity against RAMOS cells with an IC_{50} of 1.01 μM. Further compound 6k showed most potent anticancer member with values between 1.21 ± 0.12 μM against the CCRF-CEM and RAMOS cell lines. Fortunately, most of the tested hybrids showed excellent antitumor activity against RAMOS cell lines (IC_{50}: 1.01–4.93 μM). In addition, molecular docking investigation demonstrated significant binding of the ligands with both ITK and BTK targets.

4 | Methods and Materials

4.1 | Materials and Methods

All chemicals (reagent grade) used were purchased from Sigma Aldrich (India) and Avra chemicals (India). All the solvents used for the reaction are LR grade. Analytical thin-layer chromatography (TLC) was performed on precoated silica gel $60F_{254}$ plates, and visualization on TLC was achieved by UV light. Flash column chromatography was undertaken on silica gel (100−200 mesh).^{1}H NMR was recorded on 400 or 500 MHz, and chemical shifts were quoted in parts per million (ppm) referenced to 0.0 ppm for tetramethylsilane. The following abbreviations were used to describe peak splitting patterns when appropriate: br = broad, s = singlet, d = doublet, t = triplet, q = quartet, m = multiplet, dd = doublet of doublet. Coupling constants, *J*, were reported in the hertz unit (Hz). API LC-mass spectra were obtained on Agilent and Waters instruments. All the final compounds were purified on flash chromatography by using silica gel 60–120. The mobile phase was a mixture of water (0.1% formic acid) and acetonitrile. Melting points were recorded on the Buchi M-560 instrument.

4.2 | Experimental Protocol

4.2.1 | General Procedure for the Synthesis of Spiro[Azetidine-3,2'-Chroman]-4'-Ones (3a–l)

To a solution of substituted acetophenones (**1**) (1.0 eq.) in MeOH (10 Vol.) was added pyrrolidine (2.0 eq.) dropwise. Next, the corresponding ketones (**2**) (1.0 eq.) was added to the reaction

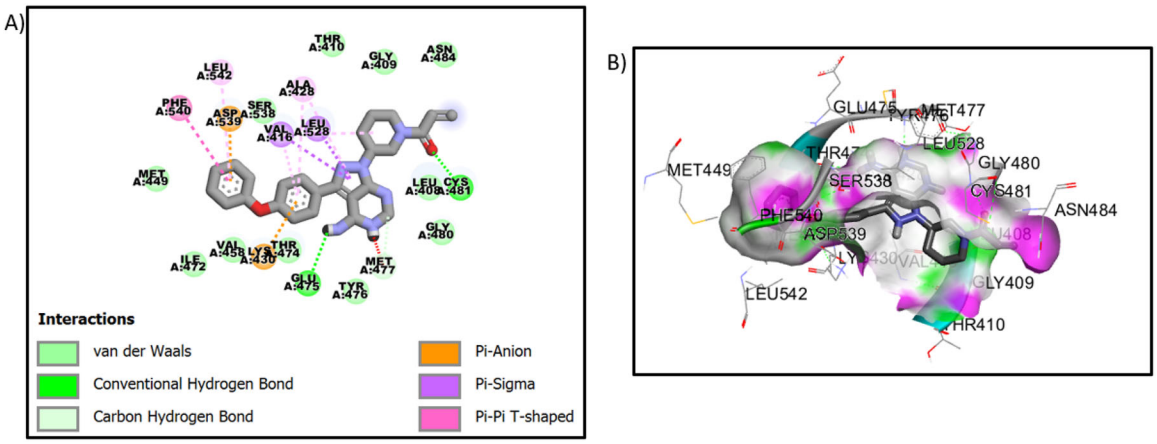

FIGURE 11 | (A) **Ibrutinib** interaction image with Protein 5P9J and (B) **Ibrutinib** showing hydrogen bond acceptor (green) and donor (pink).

mixture and stirred at 50°C for 16 h. The progress of the reaction mixture was monitored by TLC. After completion of starting material, solvent was evaporated in vacuo, and the residue was purified by Flash column chromatography on silica gel using 15% EtOAc in hexane as the eluent to afford the corresponding spiro[azetidine-3,2'-chroman]-4'-ones (**3**).

4.2.2 | General Procedure for the Synthesis of Spiro [Azetidine-3,2'-Chroman]-4'-One Intermediates (4a–l)

To a stirred solution of **3a–l** (1.0 eq.) in DCM (10 vol.) at 0°C was added trifluoroacetic acid (3.0 eq.) and reaction mixture was stirred at room temperature for 1 h. Reaction progress was monitored by TLC analysis indicates complete consumption of starting material. Reaction mixture was evaporated completely under reduced pressure to obtain crude compound. The crude was titrated with diethyl ether (2 × 30 mL) to get TFA salt of pure products of **4a–l**.

4.2.3 | General Procedure for the Synthesis of Targeted Compounds (6a–l)

To a stirred solution of intermediate **4a–l** (1.0 eq.) in DCM (20 mL) was added Et_3N (1.5 eq.) and 4-(2-(3-ethyl-4-methyl-2-oxo-2,5-dihydro-1*H*-pyrrole-1-carboxamido)ethyl)benzenesulfonyl chloride (1.5 eq.) was added to the reaction mixture at 0°C. The reaction mixture was allowed to room temperature and stirred for 16 h. The progress of the reaction was monitored by TLC. After completion of starting materials, the reaction mixture is diluted with DCM, washed with water and saturated brine solution. The organic layer was dried over Na_2SO_4, filtered and evaporated under reduced pressure to obtain crude compound. The obtained crude products were further purified with Flash chromatography using with EtOAc/Hexane to obtain title compounds **6a–l**.

4.2.3.1 | 3-Ethyl-4-methyl-2-oxo-*N*-(4-((4'-oxospiro [azetidine-3,2'-chroman]-1-yl)sulfonyl)phenethyl)-2,5-dihydro-1*H*-pyrrole-1-carboxamide (6a).

Off-white solid (205 mg, 37.5%). **^{1}H NMR** (400 MHz, $CDCl_3$): δ 8.50 (m, 1H), 7.82–7.78 (m, 3H), 7.50–7.45 (m, 3H), 7.04 (t, J = 15.20 Hz, 1H), 6.90 (d, J = 8.40 Hz, 1H), 4.18 (s, 2H), 3.95 (d, J = 9.20 Hz, 2H), 3.85 (d, J = 25.20 Hz, 2H), 3.65–3.62 (m, 2H), 3.02 (t, J = 12.40 Hz, 2H), 2.87 (s, 2H), 2.25 (q, J = 10.40 Hz, 2H), 2.04 (s, 3H), 1.05 (t, J = 13.20 Hz, 3H).; ^{13}C NMR (101 MHz, DMSO-d_6) δ 190.09, 172.40, 158.43, 152.66, 152.29, 146.30, 137.24, 132.41, 131.82, 130.36, 128.94, 126.69, 122.87, 120.70, 118.81, 75.44, 61.39, 59.05, 52.38, 47.66, 44.44, 36.98, 33.76, 16.46, 13.18.; **LC-MS** $[M+H]^+$: 524.3, purity 96.71%.

4.2.3.2 | 3-Ethyl-4-methyl-*N*-(4-((6'-methyl-4'-oxospiro [azetidine-3,2'-chroman]-1-yl)sulfonyl)phenethyl)-2-oxo-2,5-dihydro-1*H*-pyrrole-1-carboxamide (6b).

Off-white solid (51 mg, 28.6%). **^{1}H NMR** (400 MHz, $CDCl_3$): δ 8.51–8.49 (m, 1H), 7.78 (d, J = 8.00 Hz, 1H), 7.46 (d, J = 8.40 Hz, 1H), 7.30–7.27 (m, 1H), 6.79 (d, J = 8.40 Hz, 1H), 4.19 (s, 2H), 3.93 (d, J = 9.20 Hz, 2H), 3.81 (d, J = 9.20 Hz, 2H), 3.64 (q, J = 20.40 Hz, 2H), 3.01 (t, J = 14.40 Hz, 2H), 2.84 (s, 2H), 2.28 (s, 3H), 2.26–2.23 (m, 2H), 2.05 (s, 3H), 1.05 (t, J = 15.20 Hz, 3H).; ^{13}C NMR (126 MHz, DMSO-d_6) δ 190.09, 172.35, 156.45, 152.58, 152.23, 146.26, 138.02, 132.42, 131.99, 131.90, 130.34, 126.20, 120.41, 118.68, 75.37, 61.35, 52.40, 44.47, 35.73, 34.58, 25.16, 20.39, 16.48, 13.34, 13.20; **LC-MS** $[M+H]^+$: 538.3, purity 95.16%.

4.2.3.3 | *N*-(4-((7'-bromo-4'-oxospiro[azetidine-3,2'-chroman]-1-yl)sulfonyl)phenethyl)-3-ethyl-4-methyl-2-oxo-2,5-dihydro-1*H*-pyrrole-1-carboxamide (6c).

Off-white solid (109 mg, 33.2%). **^{1}H NMR** (400 MHz, $CDCl_3$): δ 8.50 (m, 1H), 7.79 (d, J = 8.40 Hz, 2H), 7.67 (d, J = 8.40 Hz, 1H), 7.47 (d, J = 8.40 Hz, 2H), 7.18 (dd, J = 8.44, 1.96 Hz, 1H), 7.09 (d, J = 2.00 Hz, 1H), 4.19 (s, 2H), 3.94 (d, J = 9.60 Hz, 2H), 3.84 (d, J = 9.60 Hz, 2H), 3.65 (q, J = 13.20 Hz, 2H), 3.02 (t, J = 14.40 Hz, 2H), 2.88 (s, 2H), 2.24 (q, J = 14.80 Hz, 2H), 2.05 (s, 3H), 1.04 (t, J = 13.20 Hz, 3H); **LC-MS** $[M+H]^+$: 604.2, purity 99.20%.

4.2.3.4 | 3-Ethyl-*N*-(4-((7'-methoxy-4'-oxospiro[azetidine-3,2'-chroman]-1-yl)sulfonyl)phenethyl)-4-methyl-2-oxo-2,5-dihydro-1*H*-pyrrole-1-carboxamide (6d).

Off-white solid (81 mg, 18.6%). **^{1}H NMR** (400 MHz, $CDCl_3$): δ 8.51–8.49 (m, 1H), 7.80–7.74 (m, 3H), 7.46 (d, J = 8.40 Hz, 2H), 6.59 (dd, J = 2.00, 8.80 Hz, 1H), 6.36 (d, J = 2.40 Hz, 1H), 4.18 (s, 2H), 3.96 (d, J = 9.20 Hz, 2H), 3.83–3.80 (m, 5H), 3.64 (q, J = 20.00 Hz, 2H), 3.01 (t, J = 14.40 Hz, 2H), 2.79 (s, 2H), 2.25 (q, J = 22.80 Hz, 2H), 2.04 (s, 3H), 1.05 (t, J = 4.80 Hz, 3H). ^{13}C NMR (101 MHz, DMSO-d_6) δ 188.34, 172.34, 166.36, 160.52, 152.55, 152.19, 146.27, 132.42,

130.36, 128.94, 114.50, 111.08, 102.07, 75.77, 61.36, 56.39, 52.39, 47.81, 33.90, 29.50, 22.58, 22.51, 16.48, 13.21.; **LC-MS** $[M+H]^+$: 554.3, purity 99.50%.

4.2.3.5 | 3-Ethyl-4-methyl-2-oxo-*N*-(4-((4-oxospiro[chromane-2,3'-pyrrolidin]-1'-yl)sulfonyl)phenethyl)-2,5-dihydro-1*H*-pyrrole-1-carboxamide (6e).

Off-white solid (51 mg, 22%). **^{1}H NMR** (400 MHz, $CDCl_3$): δ 8.53–8.50 (m, 1H), 7.82 (dd, J = 8.06, 1.82 Hz, 1H), 7.76 (d, J = 8.40 Hz, 2H), 7.43–7.39 (m, 3H), 7.01–6.98 (m, 1H), 6.45 (d, J = 8.40 Hz, 1H), 4.18 (s, 2H), 3.71–3.64 (m, 3H), 3.60 (t, J = 15.20 Hz, 1H), 3.47–3.40 (m, 1H), 3.32 (d, J = 11.60 Hz, 1H), 3.01 (t, J = 14.40 Hz, 2H), 2.78 (d, J = 4.40 Hz, 2H), 2.28–2.25 (m, 3H), 2.04 (s, 3H), 1.92–1.84 (m, 1H), 1.05 (t, J = 6.18 Hz, 3H). ^{13}C NMR (101 MHz, DMSO-d_6) δ 190.05, 172.39, 154.64, 152.73, 152.29, 146.28, 132.41, 131.84, 130.35, 128.93, 125.27, 120.81, 120.24, 107.80, 75.38, 61.28, 56.05, 52.38, 47.65, 44.42, 36.96, 35.67, 33.74, 16.46, 13.31, 13.17; **LC-MS** $[M+H]^+$: 538.3, purity 97.67%.

4.2.3.6 | 3-Ethyl-4-methyl-*N*-(4-((6-methyl-4-oxospiro[chromane-2,3'-pyrrolidin]-1'-yl)sulfonyl) phenethyl)-2-oxo-2,5-dihydro-1*H*-pyrrole-1-carboxamide (6f).

Off-white solid. (85 mg, 24.2%). **^{1}H NMR** (400 MHz, $CDCl_3$): δ 8.53–8.51 (m, 1H), 7.75 (d, J = 8.40 Hz, 2H), 7.41 (d, J = 8.00 Hz, 2H), 7.22 (dd, J = 8.40, 2.53 Hz, 1H), 6.37 (d, J = 8.40 Hz, 1H), 4.18 (s, 2H), 3.70–3.62 (m, 2H), 3.58–3.56 (m, 1H), 3.45–3.40 (m, 1H), 3.31 (d, J = 11.60 Hz, 1H), 3.03–2.99 (m, 3H), 2.75 (d, J = 3.20 Hz, 2H), 2.31 (s, 3H), 2.28–2.23 (m, 2H), 2.05 (s, 3H), 1.90–1.82 (m, 2H), 1.41 (t, J = 14.00 Hz, 1H), 1.05 (t, J = 5.20 Hz, 3H); **LC-MS** $[M+H]^+$: 552.3, purity 98.95%.

4.2.3.7 | *N*-(4-((7-bromo-4-oxospiro[chromane-2,3'-pyrrolidin]-1'-yl)sulfonyl)phenethyl)-3-ethyl-4-methyl-2-oxo-2,5-dihydro-1*H*-pyrrole-1-carboxamide (6g).

Off-white solid (135 mg, 27.7%). **^{1}H NMR** (400 MHz, $CDCl_3$): δ 8.52–8.49 (m, 1H), 7.75 (d, J = 8.00 Hz, 2H), 7.68 (d, J = 8.40 Hz, 1H), 7.45 (d, J = 8.40 Hz, 2H), 7.14 (dd, J = 8.42, 1.67 Hz, 1H), 6.54 (d, J = 1.20 Hz, 1H), 4.18 (s, 2H), 3.70–3.64 (m, 2H), 3.62–3.58 (m, 2H), 3.43–3.37 (m, 1H), 3.34 (d, J = 11.60 Hz, 1H), 3.05 (t, J = 14.80 Hz, 2H), 2.78 (s, 2H), 2.28–2.21 (m, 3H), 1.95–1.87 (m, 1H), 1.05 (t, J = 15.20 Hz, 3H); **LC-MS** $[M+H]^+$: 618.1, purity 96.44%.

4.2.3.8 | 3-Ethyl-*N*-(4-((7-methoxy-4-oxospiro[chromane-2,5'-oxazolidin]-3'-yl)sulfonyl)phenethyl)-4-methyl-2-oxo-2,5-dihydro-1*H*-pyrrole-1-carboxamide (6h).

Off-white solid (25 mg, 29%). **^{1}H NMR** (400 MHz, $CDCl_3$): δ 8.4 (m, 1H), 7.78–7.76 (m, 2H), 7.42 (d, J = 8.40 Hz, 2H), 6.56 (dd, J = 8.82, 2.40 Hz, 1H), 5.99 (d, J = 2.40 Hz, 1H), 4.18 (s, 2H), 3.82 (s, 3H), 3.71 (d, J = 10.00 Hz, 1H), 3.66 (q, J = 14.40 Hz, 2H), 3.54–3.46 (m, 2H), 3.27 (d, J = 11.60 Hz, 1H), 3.00 (t, J = 14.80 Hz, 2H), 2.71 (d, J = 5.20 Hz, 1H), 2.29–2.23 (m, 3H), 2.05 (s, 3H), 1.89–1.81 (m, 1H), 1.05 (t, J = 15.20 Hz, 3H).; **LC-MS** $[M+H]^+$: 568.3, purity 95.09%.

4.2.3.9 | 3-Ethyl-4-methyl-2-oxo-*N*-(4-((4-oxospiro[chromane-2,4'-piperidin]-1'-yl)sulfonyl)phenethyl)-2,5-dihydro-1*H*-pyrrole-1-carboxamide (6i).

Off-white solid (210 mg, 40%). **^{1}H NMR** (400 MHz, $CDCl_3$): δ 8.51 (t, J = 10.80 Hz, 1H), 7.83 (dd, J = 7.80, 1.69 Hz, 1H), 7.72 (dd, J = 8.00, 1.98 Hz, 2H), 7.45–7.41 (m, 3H), 7.00–6.96 (m, 1H), 6.81 (dd, J = 8.40, Hz, 1H), 4.19 (s, 2H), 3.66–3.56 (m, 4H), 3.00 (t, J = 14.40 Hz, 2H), 2.85–2.79 (m, 2H), 2.68 (s, 2H), 2.26 (q, J = 7.60 Hz, 2H), 2.10 (dd, J = 12.40, Hz, 2H), 2.05 (s, 3H), 1.82–1.78 (m, 2H), 1.05 (t, J = 15.20 Hz, 3H). ^{13}C NMR (101 MHz, DMSO-d_6) δ 196.45, 177.11, 163.36, 157.33, 156.97, 150.28, 141.75, 138.64, 137.19, 134.97, 132.78, 131.12, 126.50, 123.35, 81.95, 63.94, 57.14, 49.31, 41.85, 40.45, 37.81, 27.22, 21.23, 18.09, 17.96, 8.88. **LC-MS** $[M+H]^+$: 552.3, purity 98.09%.

4.2.3.10 | 3-Ethyl-4-methyl-*N*-(4-((6-methyl-4-oxospiro[chromane-2,4'-piperidin]-1'-yl)sulfonyl)phenethyl)-2-oxo-2,5-dihydro-1*H*-pyrrole-1-carboxamide (6j).

Off-white solid (100 mg, 29%). **^{1}H NMR** (400 MHz, $CDCl_3$): δ 8.53–8.50 (m, 1H), 7.71 (dd, J = 8.12, 1.63 Hz, 2H), 7.42 (d, J = 8.40 Hz, 2H), 7.25–7.23 (m, 1H), 6.70 (d, J = 8.40 Hz, 1H), 4.19 (s, 2H), 3.64 (q, J = 20.40 Hz, 2H), 3.57–3.55 (m, 2H), 3.00 (t, J = 14.80 Hz, 2H), 2.84–2.78 (m, 2H), 2.65 (s, 2H), 2.29–2.23 (m, 5H), 2.10–2.07 (m, 2H), 2.05 (s, 3H), 1.80–1.72 (m, 2H), 1.05 (t, J = 14.80 Hz, 3H). ^{13}C NMR (101 MHz, DMSO-d_6) δ 190.04, 172.35, 166.29, 160.65, 152.57, 152.21, 145.51, 134.04, 132.44, 130.24, 128.00, 117.36, 114.54, 109.85, 101.91, 77.57, 59.14, 56.18, 52.37, 47.76, 44.53, 33.83, 33.20, 29.39, 29.24, 22.45, 16.46, 13.19.; **LC-MS** $[M+H]^+$: 566.4, purity 97.49%.

4.2.3.11 | *N*-(4-((7-bromo-4-oxospiro[chromane-2,4'-piperidin]-1'-yl)sulfonyl)phenethyl)-3-ethyl-4-methyl-2-oxo-2,5-dihydro-1*H*-pyrrole-1-carboxamide (6k).

Off-white solid (110 mg, 34.3%). **^{1}H NMR** (400 MHz, $CDCl_3$): δ 8.50–8.49 (m, 1H), 7.77–7.67 (m, 3H), 7.43 (d, J = 8.40 Hz, 2H), 7.12 (dd, J = 8.45, 1.60 Hz, 1H), 7.03 (s, 1H), 4.18 (s, 2H), 3.67–3.58 (m, 5H), 3.01 (t, J = 14.40 Hz, 2H), 2.84–2.77 (m, 2H), 2.67 (s, 2H), 2.24 (q, J = 12.80 Hz, 3H), 2.10–2.02 (m, 5H), 1.83–1.75 (m, 2H), 1.04 (t, J = 5.20 Hz, 3H); **LC-MS** $[M+H]^+$: 632.3, purity 96.94%.

4.2.3.12 | 3-Ethyl-*N*-(4-((7-methoxy-4-oxospiro[chromane-2,4'-piperidin]-1'-yl)sulfonyl)phenethyl)-4-methyl-2-oxo-2,5-dihydro-1*H*-pyrrole-1-carboxamide (6l).

Off-white solid (110 mg, 43.5%). **^{1}H NMR** (400 MHz, $CDCl_3$): δ 8.51 (m, 1H), 7.78 (d, J = 8.80 Hz, 1H), 7.72 (d, J = 8.40 Hz, 1H), 7.42 (d, J = 8.13 Hz, 2H), 6.54 (dd, J = 8.81, 2.40 Hz, 1H), 6.22 (d, J = 42.40 Hz, 1H), 4.18 (s, 2H), 3.78 (s, 3H), 3.66–3.60 (m, 2H), 3.57–3.54 (m, 2H), 2.99 (t, J = 14.40 Hz, 2H), 2.89–2.83 (m, 2H), 2.62 (s, 2H), 2.26 (q, J = 12.40 Hz, 2H), 2.11–2.05 (m, 2H), 2.03 (s, 3H), 1.81–1.74 (m, 2H), 1.05 (t, J = 5.96 Hz, 3H).; **LC-MS** $[M+H]^+$: 582.3, purity 97.45%.

4.3 | Cytotoxicity Assay

The cytotoxic effects of the synthesized compounds were evaluated using the 3-(4,5-dimethylthiazol-2-yl)-5-(3-carboxymethoxyphenyl)-2-(4-sulfophenyl)-2H-tetrazolium (MTS) assay following 72 h of compound treatment [38, 39]. Cell viability was determined using the CellTiter 96 AQueous One Solution Cell Proliferation Assay kit (Promega, USA) according to the validated protocol routinely employed in our laboratory and as previously described [42–44]. Human cell lines were obtained from ATCC (Middlesex, UK) or DSMZ (Braunschweig, Germany) and maintained at 37°C in a humidified atmosphere containing 5% CO_2 using the recommended culture media supplemented with 10% fetal calf serum, 100 U/mL penicillin, 100 µg/mL

streptomycin, 2 mM glutamine, 1 mM sodium bicarbonate, 1 mM sodium pyruvate, and 20 mM HEPES. Cell lines were routinely authenticated and screened for mycoplasma contamination.

The cancer and non-cancer cell lines with different reported ITK/BTK expression profiles were used such as, HCT116, HCT116 p53−/−, U2OS, A549, Jurkat, CCRF-CEM, RAMOS, K562, MRC-5, and BJ. All assays included DMSO-treated cells as negative controls, while ibrutinib was used as an internal reference compound and evaluated under identical assay conditions. Test compounds (0–50 μM) and ibrutinib (0–100 nM) were serially diluted in reaction buffer containing 10% DMSO and dispensed (1 μL per well) into 384-well plates, maintaining a final DMSO concentration ≤ 0.5% (*v*/*v*) in all assay wells. Experiments were performed using a robotic high-throughput screening platform (HighResBio, Boston, MA, USA) with three biological and three technical replicates. Dose–response curves were generated and IC_{50} values were determined by nonlinear regression analysis using Dotmatics software (San Diego, CA, USA). The therapeutic index (TI) was calculated as the ratio of IC_{50} values in fibroblast cells (BJ or MRC-5) to those in Jurkat cells. For compounds showing no measurable cytotoxicity in fibroblasts up to 50 μM (IC_{50} > 50 μM), TI values were reported as not determined (n.d.), and 50 μM was considered the upper assay limit for estimation. All experiments were performed in three biological replicates and three technical replicates. IC_{50} values were calculated by nonlinear regression analysis using GraphPad Prism software and expressed as the concentration required to reduce cell viability by 50%.

4.4 | Preparation of Protein/Receptor and Compounds

PyRx software with Autodock Vina was used to conduct molecular docking investigations [40, 41]. The Protein was downloaded in#x000A0;.pdb format from the protein data bank database (www.rcsb.org), which is maintained by the Research Collaboratory for Structural Bioinformatics (RCSB). One chain in each protein was chosen as the study's target, and the AutoDock tool was used to prepare the protein. The native ligand, non-interacting ions, and water molecules were all removed from the crystal structures. A grid box for BTK/ITK with the dimensions *X*: 2.866, *Y*: 8.84, *Z*: 14.89 Å, and the size of the grid box-22 × 22 × 22, was identified as the protein target docking site [42, 43]. To reduce the stress on the crystal structure and enable the protein to be used in the AutoDock docking simulation tool, the missing hydrogens were added. The Chem Draw was used to illustrate chemicals **6a–l**. They were converted to pdbqt files and the structure was minimized using universal forcefield. The 4M15 and 5P9J were used to to predict the anticancer activity of ITK and BTK, respectively. The protein's cognate ligand was selected as the binding site in order to analyze the binding affinity.

4.5 | SwissADME

Swiss ADME (www.swissadme.ch) is a free online tool which evaluates the accessibility of small molecules' medicinal chemistry in addition to their pharmacokinetics and drug-likeness. This application offers free access to a collection of fast yet highly accurate predictive models for pharmacokinetics and physicochemical characteristics, including proprietary sophisticated techniques like the Bioavailability Radar, iLOGP, and BOILED-Egg.

4.6 | Discovery Studio

The Discovery Studio assists in determining the type of contact, bond lengths, and interactions between the active sites in the target and ligand conformation. One special, centralized, and convenient graphical interface for effective drug design and protein modelling.

Author Contributions

Ramesh Reddy Mudda: formal analysis, methodology, investigation, writing – original draft. Prof. **Rambabu Gundla:** software, funding acquisition, project administration, supervision. **Dr. Vikram Basava:** resources, supervision, writing – review and editing. **Dr. Baji Baba Shaik:** data curation and writing – original draft. **Dr. Vani Madhuri Velavalapalli:** software. **Dr. Ramanaiah Chennuru:** formal analysis, validation. **Dr. Soňa Gurská:** data curation and validation. **Dr. Viswanath Das:** conceptualization, funding acquisition, resources, writing – review and editing. **Dr. Naresh Kumar Katari:** visualization, writing – review and editing.

Acknowledgments

The authors would like to thank GITAM university for all necessary facilities.

Conflicts of Interest

The authors declare no conflicts of interest.

Data Availability Statement

The data that support the findings of this study are available in the Supporting Information of this article.

References

1. Z. Wu, F. Xia, and R. Lin, "Global Burden of Cancer and Associated Risk Factors in 204 Countries and Territories, 1980–2021: A Systematic Analysis for the GBD 2021," *Journal of Hematology & Oncology* 17 (2024): 119, https://doi.org/10.1186/s13045-024-01640-8.

2. C. Weiss, "One in Four Dies of Cancer. Questions About the Epidemiology of Malignant Tumours," in *Ethical Challenges in Cancer Diagnosis and Therapy* 218 (2021): 15–29, https://doi.org/10.1007/978-3-030-63749-1_2.

3. U. Anand, A. Dey, A. K. S. Chandel, et al., "Cancer Chemotherapy and Beyond: Current Status, Drug Candidates, Associated Risks and Progress in Targeted Therapeutics," *Genes & Diseases* 10 (2022): 1367–1401, https://doi.org/10.1016/j.gendis.2022.02.007.

4. F. Davodabadi, S. F. Sajjadi, M. Sarhadi, et al., "Cancer Chemotherapy Resistance: Mechanisms and Recent Breakthrough in Targeted Drug Delivery," *European Journal of Pharmacology* 958 (2023): 176013, https://doi.org/10.1016/j.ejphar.2023.176013.

5. A. Zafar, S. Khatoon, M. J. Khan, J. Abu, and A. Naeem, "Advancements and Limitations in Traditional Anti-Cancer Therapies: A Comprehensive Review of Surgery, Chemotherapy, Radiation Therapy, and Hormonal Therapy," *Discover Oncology* 16 (2025): 607, https://doi.org/10.1007/s12672-025-02198-8.

6. V. K. Dhiman, M. Kumari, and D. Singh, "Chemoresistance: Chemoresistance: The Hidden Barrier in Cancer Treatment," *Cancer Pathogenesis and Therapy* 4 (2025): 98–109, https://doi.org/10.1016/j.cpt.2025.07.001.

7. Global Cancer Observatory, Global Cancer Observatory, Iarc.fr. (2020), https://gco.iarc.fr/.

8. World Health Organization, *Global Cancer Burden Growing, Amidst Mounting Need for Services* (WHO, 2024), https://www.who.int/news/item/01-02-2024-global-cancer-burden-growing–amidst-mounting-need-for-services.

9. F. Bray, M. Laversanne, H. Sung, et al., "Global Cancer Statistics 2022: GLOBOCAN Estimates of Incidence and Mortality Worldwide for 36 Cancers in 185 Countries," *CA: A Cancer Journal for Clinicians* 74 (2024): 229–263, https://doi.org/10.3322/caac.21834.

10. M. Elmadani, P. O. Mokaya, E. K. K. Ahmed, S. Klara, and M. Orsolya, "Cancer Burden in Europe: A Systematic Analysis of the GLOBOCAN Database (2022)," *BMC Cancer* 25 (2025), 447, https://doi.org/10.1186/s12885-025-13862-1.

11. R. L. Siegel, T. B. Kratzer, A. N. Giaquinto, H. Sung, and A. Jemal, "Cancer Statistics, 2025," *CA: A Cancer Journal for Clinicians* 75 (2025): 10–45, https://doi.org/10.3322/caac.21871.

12. J. K. Triantafillidis, G. Nasioulas, and P. A. Kosmidis, "Colorectal Cancer and Inflammatory Bowel Disease: Epidemiology, Risk Factors, Mechanisms of Carcinogenesis and Prevention Strategies," *Anticancer Research* 29 (2009): 2727–2737.

13. D. Basavaraja, S. V. Doddamani, C. S. Athira, et al., "Spiro-Heterocycles: Recent Advances in Biological Applications and Synthetic Strategies," *Tetrahedron* 173 (2025): 134468, https://doi.org/10.1016/j.tet.2025.134468.

14. R. S. Kumar, A. I. Almansour, N. Arumugam, F. Mohammad, and R. R. Kumar, "In Vitro Mechanistic Exploration of Novel Spiropyrrolidine Heterocyclic Hybrids as Anticancer Agents," *Frontiers in Chemistry* 8 (2020): 465, https://doi.org/10.3389/fchem.2020.00465.

15. L. L. Romero-Hernández, P. Merino-Montiel, S. Meza-Reyes, et al., "Synthesis of Unprecedented Steroidal Spiro Heterocycles as Potential Antiproliferative Drugs," *European Journal of Medicinal Chemistry* 143 (2017): 21–32, https://doi.org/10.1016/j.ejmech.2017.10.063.

16. A. Arya, K. Rana, and M. Kumar, "A Facile Synthesis and Anticancer Activity Evaluation of Spiro Analogues of Benzothiazolylchromeno/Pyrano Derivatives," *Letters in Drug Design & Discovery* 11 (2013): 594–600, https://doi.org/10.2174/15701808116661312100009003.

17. K. Sai Chaitanya, P. Gupta, S. Chitti, et al., "Development and Biological Evaluation of Novel Spiro 4-Chromanones as Potent Quorum Sensing Inhibitors," *Journal of Chemistry* 2024 (2024): 8227205, https://doi.org/10.1155/2024/8227205.

18. S.-S. Liu, D. Zhang, T. Zhang, et al., "Novel Spiro[Chromanone-2,4′-Piperidine]-4-One Derivatives as Potential Inhibitors of Fatty Acid Synthesis in Pathogens: Design, Synthesis, and Biological Evaluation," *European Journal of Medicinal Chemistry* 250 (2023): 115215, https://doi.org/10.1016/j.ejmech.2023.115215.

19. A. S. Karandeeva, N. A. Bogdanova, M. V. Kabanova, et al., "Diastereoselective Synthesis and Biological Evaluation of Spiro[chromane-2,4′-Pyrimidin]-2′(3′H)-Ones as Novel Antimicrobial and Antioxidant Agents," *Molecules* 30 (2025): 2954, https://doi.org/10.3390/molecules30142954.

20. J. M. Hwang, T.-H. Oh, T. Kaneko, et al., "Design, Synthesis, and Structure–Activity Relationship Studies of Tryptanthrins as Antitubercular Agents," *Journal of Natural Products* 76 (2013): 354–367, https://doi.org/10.1021/np3007167.

21. S. Chitti, S. Pulya, A. Nandikolla, et al., "Design, Synthesis and Biological Evaluation of 7–(5–((Substituted—Amino)-Methyl)-Thiophen–2–Yl)-Spiro-[Chroman–2,4′–Piperidin]–4–One Hydrochloride Analogues as Anticancer Agents," *Bioorganic Chemistry* 112 (2021): 104865, https://doi.org/10.1016/j.bioorg.2021.104865.

22. S. Emami and Z. Ghanbarimasir, "Recent Advances of Chroman-4-One Derivatives: Synthetic Approaches and Bioactivities," *European Journal of Medicinal Chemistry* 93 (2015): 539–563, https://doi.org/10.1016/j.ejmech.2015.02.048.

23. S. Nakka, S. Sengar, K. Sai Chaitanya, et al., "Design and Synthesis of Novel Spiro [Chromane-2,4′-Piperidin]-4-One Derivatives: Anti-Proliferative Investigation and Molecular Docking Studies," *Asian Journal of Organic Chemistry* 14 (2024): e202400604, https://doi.org/10.1002/ajoc.202400604.

24. M. Varasi, F. Thaler, A. Abate, et al., "Discovery, Synthesis, and Pharmacological Evaluation of Spiropiperidine Hydroxamic Acid Based Derivatives as Structurally Novel Histone Deacetylase (HDAC) Inhibitors," *Journal of Medicinal Chemistry* 54 (2011): 3051–3064, https://doi.org/10.1021/jm200146u.

25. "Synthesis and Anticancer Screening of Novel Spiro[Synthesis and Anticancer Screening of Novel Spiro[Chroman-2,4'- Piperidin]-4-One Derivatives With Apoptosis-Inducing Activity," *Journal of Applied Pharmaceutical Science* 8 (2018): e202400604, https://doi.org/10.7324/japs.2018.8102.

26. G. Culletta, M. Tutone, M. Zappalà, and A. M. Almerico, "Sulfonamide Moiety as "Molecular Chimera" in the Design of New Drugs," *Current Medicinal Chemistry* 30 (2023): 128–163, https://doi.org/10.2174/0929867329666220729151500.

27. A. Ovung and J. Bhattacharyya, "Sulfonamide Drugs: Structure, Antibacterial Property, Toxicity, and Biophysical Interactions," *Biophysical Reviews* 13 (2021): 259–272, https://doi.org/10.1007/s12551-021-00795-9.

28. T. C. S. Ho, A. H. Y. Chan, and A. Ganesan, "Thirty Years of HDAC Inhibitors: 2020 Insight and Hindsight," *Journal of Medicinal Chemistry* 63 (2020): 12460–12484, https://doi.org/10.1021/acs.jmedchem.0c00830.

29. A. Ashkenazi, W. J. Fairbrother, J. D. Leverson, and A. J. Souers, "From Basic Apoptosis Discoveries to Advanced Selective BCL-2 Family Inhibitors," *Nature Reviews Drug Discovery* 16 (2017): 273–284, https://doi.org/10.1038/nrd.2016.253.

30. P. Hamberg, J. Verweij, and S. Sleijfer, "(Pre-)Clinical Pharmacology and Activity of Pazopanib, a Novel Multikinase Angiogenesis Inhibitor," *Oncologist* 15 (2010): 539–547, https://doi.org/10.1634/theoncologist.2009-0274.

31. A. Daina, O. Michielin, and V. Zoete, "SwissADME: A Free Web Tool to Evaluate Pharmacokinetics, Drug-Likeness and Medicinal Chemistry Friendliness of Small Molecules," *Scientific Reports* 7 (2017): 1–13, https://doi.org/10.1038/srep42717.

32. J. Huuskonen, D. J. Livingstone, and D. T. Manallack, "Prediction of Drug Solubility From Molecular Structure Using a Drug-Like Training Set," *SAR and QSAR in Environmental Research* 19 (2008): 191–212, https://doi.org/10.1080/10629360802083855.

33. M. V. Varma, Y. Lai, and A. F. El-Kattan, "Molecular Properties Associated With Transporter-Mediated Drug Disposition," *Advanced Drug Delivery Reviews* 116 (2017): 92–99, https://doi.org/10.1016/j.addr.2017.05.014.

34. C. A. Lipinski, F. Lombardo, B. W. Dominy, and P. J. Feeney, "Experimental and Computational Approaches to Estimate Solubility and Permeability in Drug Discovery and Development Settings," *Advanced Drug Delivery Reviews* 64 (2012): 4–17, https://doi.org/10.1016/j.addr.2012.09.019.

35. D. F. Veber, S. R. Johnson, H.-Y. Cheng, B. R. Smith, K. W. Ward, and K. D. Kopple, "Molecular Properties That Influence the Oral Bioavailability of Drug Candidates," *Journal of Medicinal Chemistry* 45 (2002): 2615–2623, https://doi.org/10.1021/jm020017n.

36. P. D. Leeson and A. M. Davis, "Time-Related Differences in the Physical Property Profiles of Oral Drugs," *Journal of Medicinal Chemistry* 47 (2004): 6338–6348, https://doi.org/10.1021/jm049717d.

37. L. Guan, H. Yang, Y. Cai, et al., "ADMET-Score—A Comprehensive Scoring Function for Evaluation of Chemical Drug-Likeness," *MedChemComm* 10 (2019): 148–157, https://doi.org/10.1039/c8md00472b.

38. J. McCauley, A. Zivanovic, and D. Skropeta, "Bioassays for Anticancer Activities," *Methods in Molecular Biology* 1055 (2013): 191–205, https://doi.org/10.1007/978-1-62703-577-4_14.

39. C. Sanjai, S. S. Hakkimane, B. R. Guru, and S. L. Gaonkar, "A Comprehensive Review on Anticancer Evaluation Techniques," *Bioorganic Chemistry* 142 (2024): 106973, https://doi.org/10.1016/j.bioorg.2023.106973.

40. F. Houshmand and S. Houshmand, "Potentially Highly Effective Drugs for COVID-19: Virtual Screening and Molecular Docking Study Through PyRx-Vina Approach," *Frontiers in Health Informatics* 12 (2023): 150, https://doi.org/10.30699/fhi.v12i0.478.

41. S. Dallakyan and A. J. Olson, "Small-Molecule Library Screening by Docking With PyRx," *Methods in Molecular Biology* 1263 (2014): 243–250, https://doi.org/10.1007/978-1-4939-2269-7_19.

42. R. R. Mudda, V. Basava, R. Gundla, et al., "New Molecular Hybrids of Spirochromanone and Carbamide: Design, Synthesis, Docking and In Vitro Anticancer Studies," *Journal of the Indian Chemical Society* 102 (2025): 102177, https://doi.org/10.1016/j.jics.2025.102177.

43. G. Mudasani, N. K. Rampeesa, S. R. Anugu, et al., "Design, Synthesis, and Biological Evaluation of Novel Azaspirooxindolinone Derivatives as Potent Inhibitors of ITK and BTK-Dependent Cancers," *Bioorganic & Medicinal Chemistry* 121 (2025): 118116, https://doi.org/10.1016/j.bmc.2025.118116.

44. S. Tangallapalli, R. Gundla, K. Paidikondala, et al., "Design, Synthesis, and Biological Evaluation of Novel 3-Oxo-2,3-Dihydropyridazine Derivatives as Interleukin-2-Inducible T-Cell Kinase (ITK) Inhibitors," *RSC Advances* 15 (2025): 47565–47586, https://doi.org/10.1039/d5ra06565h.

Supporting Information

Additional supporting information can be found online in the Supporting Information section.

Supporting File 1: slct74187-sup-0001-SuppMat.docx